Int. J. Electrochem. Sci., 12 **(2017)** 10269 – 10278, doi: 10.20964/2017.11.15

International Journal of
ELECTROCHEMICAL
SCIENCE
www.electrochemsci.org

A Sensitive Hydrazine Electrochemical Sensor Based on Ag-Ni Alloy/Reduced Graphene Oxide Composite

Zuchao Meng[*], *Bin Liu, Mao Li*

College of Chemistry and Chemical Engineering, Xi'an shiyou University, Xi'an Shaanxi 710065, China
[*]E-mail: cmeng@xsyu.edu.cn

Received: 15 July 2017 / *Accepted:* 23 august 2017 / *Published:* 12 October 2017

A sensitive hydrazine sensor based on Ag-Ni/reduced graphene oxide (rGO) has been prepared via an electrodepositing method. The Ag-Ni/rGO composite was characterized by scanning electron microscopy (SEM), energy- dispersive X-ray spectroscopy analysis (EDS) and X-ray diffraction (XRD). The Ag-Ni/rGO composite had good electrocatalytic activity for hydrazine oxidation. The electrochemical behaviour of Ag-Ni/rGO for hydrazine oxidation was also explored. When the concentration of hydrazine changed from 1.0μM to 1.05 mM, the oxidation peak currents linearly increased. The detection limit was 0.3μM (S/N=3). The sensor based on Ag-Ni/rGO was also used to determine the hydrazine concentration in waste water and the results were satisfactory. The sensor based on Ag-Ni/rGO was easily fabricated and had a high stability, wide linear range, low cost and potential applications for real sample analysis.

Keywords: reduced graphene oxide, Ag-Ni alloy, hydrazine, electrodeposition, sensor

1. INTRODUCTION

Hydrazine and its derivatives have been widely used in industry, agriculture, and military applications. Hydrazine has been applied as an insecticide, plant-growth regulators, propellants, and pharmaceuticals and is a carcinogenic and hepatotoxic substance [1-2], Some adverse health effect, such as DNA damage [3], blood abnormalities, and irreversible deterioration of the nervous system [4], can be produced by hydrazine. Thus, suitable analytical methods for the determination of hydrazine in biological and industrial processes are needed. Due to its high toxicity and carcinogenicity, the detection of hydrazine has attracted more attention. Many methods and techniques, such as ion chromatography, optical chemical sensors, flow injection analysis, chemiluminescence, and various types of spectroscopy, have been established for the detection of hydrazine [5-10]. Compared with

other methods, electrochemical techniques are economical, simple, sensitive, and rapid for hydrazine determination [11, 12].

In recent years, increasing attention has been paid to alloys, because alloys can preserve the properties of each component and potentially result in synergistic effects from cooperative interactions. As a result, surface areas can be increased, electrocatalytic activities and biocompatibilities can be enhanced, and electron transfer rates can be promoted [13]. Au-Ag [14], Au-Pt [15], Au-Pd [16], Pd-Cu [17], Pt-Pb [18] and Ni-Pt [19] have been used to fabricate electrochemical sensors. Furthermore, many graphene-supported alloys, which show high electrocatalytic activities and selectivities for applications in electrochemical sensing, have been reported. Pt_3M (M=Co, Cr) alloy/graphene was synthesized via an ethylene glycol reduction method, and it showed high activity for the oxygen reduction reaction [20]. A Au-Pd/GO composite was prepared via electrochemical reduction, and it showed a high biocompatibility and electroactive surface area and enhanced the electron transfer kinetics of the oxygen reduction reaction[21]. The Pt-Ag alloy/graphene composite was prepared via the self-organization of Au@PtAg nanorods on graphene, and it showed catalytic activity and a high stability for the electro-oxidation of methanol [22].

Currently, many approaches such as the gas condensation method, heat treatment method, γ-radiation method, radiolysis and chemical reduction have been reported for the synthesis of Ag-Ni alloy [23-27]. In this work, we present a facile method to prepare an Ag-Ni alloy on rGO via electrodeposition for the first time. Due to the synergetic effects of Ag-Ni alloy and rGO, the fabricated sensor based on the Ag-Ni/rGO composite exhibited a high electrocatalytic activity and sensitivity for hydrazine detection.

2. EXPERIMENTAL

2.1. Apparatus

A Model CHI660E electrochemistry workstation (Chenhua Instruments Co., Ltd., Shanghai, China) was used for all the electrochemical techniques. A three-electrode system was used, and a standard saturated calomel electrode (SCE), platinum wire electrode and modified glassy carbon electrode (GCE, Φ=3 mm) served as the reference electrode, the auxiliary electrode, and working electrode, respectively. All the electrochemical experiments were conducted at room temperature (25°C). Scanning electron microscopy (SEM) and energy dispersive spectroscopy (EDS) measurements were performed using a JSM-6700F scanning electron microscope (Japan Electron Company, Japan). The X-ray diffraction (XRD) measurements were performed using a Rigaku X-ray diffractometer (Ricoh Company Ltd., Tokyo, Japan).

2.2. Reagents

Graphite powder, silver nitrate and hydrazine hydrate were purchased from Sinopharm Chemical Reagent Co., Ltd. Nickel nitrate was purchased from Tianjin Fuchen Chemical Reagent Company. Potassium permanganate was purchased from Tianjin Kermel Chemical Reagent Co., Ltd.

A 0.1 M solution of NaOH was used as the supporting electrolyte. All other reagents were of analytical grade, and all the solutions were prepared with water purified in a Milli-Q Millipore system.

2.3. Preparation of rGO

GO was prepared via the Hummers method and purified [28, 29]. Graphite (10 g) and $NaNO_3$ (5 g) were mixed with 230 mL of H_2SO_4 in a 5 L beaker. The mixture was stirred for 30 min in an ice bath. While maintaining the vigorous stirring, $KMnO_4$ (30 g) was added to the suspension. The rate of addition was carefully controlled to maintain the reaction temperature at 35°C for 30 min.

As the reaction progressed, the mixture gradually became pasty, and the colour became light brownish. Next, 3.5 L of H_2O was slowly added to the paste with vigorous agitation. Then, 30% H_2O_2 was gradually added to the mixture until the colour changed to yellow. For purification, the mixture was washed by rinsing and centrifugation with 5% HCl and then deionized water several times. After filtration and drying under a vacuum, GO was obtained as a grey powder.

rGO was subsequently obtained via a typical experiment. The GO (50 mg) was dispersed in 50 mL of deionized water by ultrasonication for 40 min. Then, 0.5 mL of hydrazine monohydrate was added, and the mixture was stirred (400 rpm) at 80°C for 10 h. Finally, black rGO was obtained as a black powder by filtration washing.

2.4. Preparation of Ag-Ni/rGO/GCE

The GCE was polished before each experiment with 0.3, and 0.05 μm α-alumina powders in sequence, ultrasonicated in 1:1 HNO_3, ethanol, and doubly distilled water, and allowed to dry at room temperature. The rGO (3 mg) was dispersed in DMF by ultrasonication to obtain a 0.3 mg/mL suspension. Then, 10μl of the 0.3 mg/mL rGO solution was dropped onto the surface of a pretreated GCE and dried in air to obtain the rGO modified electrode (rGO/GCE). The Ag-Ni/rGO/GCE was prepared by electrodepositing Ag-Ni alloy on the rGO/GCE with a 0.1 mol/L$AgNO_3$ + 0.05 mol/L $Ni(NO_3)_2$ + 0.1 mol/L KNO_3 solution via cyclic scanning from 0 V to -1.0 V for different cycles at a scan rate of 50 mV s^{-1}. As a comparison, both Ag/rGO/GCE and Ni/rGO/GCE were fabricated following the same procedure in the absence of Ni or Ag, respectively.

2.5. Experimental procedures

Cyclic voltammetry (CV) and linear sweep voltammetry (LSV) were performed in a cell containing 20 mL of 0.1 M NaOH at room temperature. All solutions were deoxygenated by bubbling highly pure nitrogen for 20 min and were maintained under a nitrogen atmosphere during measurements.

3. RESULTS AND DISCUSSION

3.1. Characterization of Ag-Ni/rGO composite

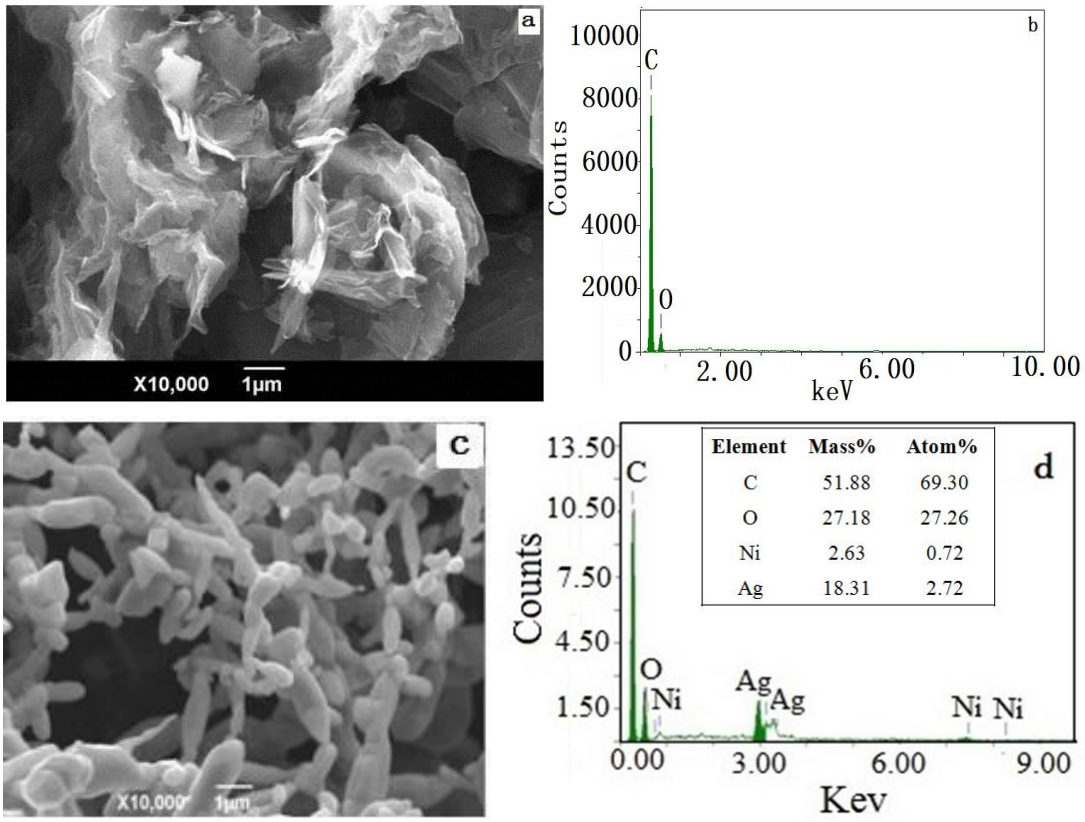

Figure 1. SEM of the rGO (a) and Ag-Ni/rGO composite (c), EDS analysis of the rGO (b) and Ag-Ni/rGO composite (d)

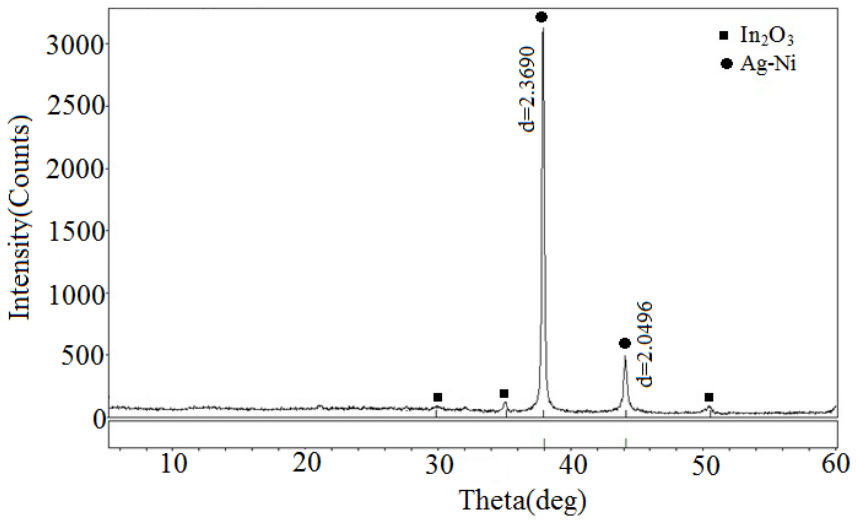

Figure 2. XRD patterns of the Ag-Ni/rGO composite on the ITO

The typical SEM of rGO is showed in Fig. 1a, and rGO has a sheet-like structure with thin layers, and wrinkled edges. The presence of C and O can be seen from the EDS analysis (Fig. 1b).

From Fig. 1c, we can see that the stick-like Ag-Ni alloy formed on the surface of the rGO and the size of the Ag-Ni was large. The EDS analysis (Fig. 1d) showed the presence of C, Ag and Ni (The O came from rGO). The result demonstrated that the Ag-Ni composite was successfully electrodeposited on the rGO.

The size of the stick-like Ag-Ni alloy was larger than the nanometer scale. In general, when metals are on the nanometer scale, the metals are inclined to nucleate and become multiply twinned particles with surfaces bound by the lowest-energy facets [30]. The larger size of the Ag-Ni alloy may be attributed to the fact that small Ag-Ni nanoparticles show a strong tendency to agglomerate due to their high surface energy and the high surface tension of the ultrafine nanoparticles [31].

The XRD patterns of Ag-Ni/rGO are shown in Fig. 2. The XRD peak for rGO at 24° could not be clearly seen which may be due to the high intensity of metal peaks over the rGO [32]. The weak diffraction peaks at 30°, 35° and 51° belong to In_2O_3 (JCPDS No. 65-3170). In the alloy compositions, the two peaks located at 38.0° and 44.1° were similar to the diffraction from Ag metal (JCPDS No. 04-0783). The peak at 52.15° corresponding to Ni metal was not observed [33-36]. The results showed that Ni atoms only grow inside the Ag lattice and form the Ag-Ni alloy [37]. The reason for this is that the redox potential of Ag^+/Ag (+0.8 V) is higher than that of Ni^{2+}/Ni (+0.246 V), and the Ag metal ions can be reduced earlier than the Ni^{2+} ions to provide lattice sites for the Ni^0 atom nucleation and stabilization.

The CVs for Ag-Ni/rGO/GCE in 0.1 M NaOH in the absence (E) and presence of 0.1 mM hydrazine (F) are shown in Fig. 3. For comparison, the behaviors of Ag/rGO/GCE (C), Ni/rGO/GCE (D), rGO/GCE (B) and GCE (A) in presence of 0.1 mM hydrazine are also presented. It can be seen that Ag-Ni/rGO had a higher current response for the electrocatalytical oxidation of hydrazine than the other materials, which might be attributed to the large area of Ag-Ni/rGO and the good synergetic effect between the Ag-Ni alloy and rGO. According to previous reports [38], the electrochemical mechanism for hydrazine oxidation on the Ag-Ni/rGO/GCE is $N_2H_4 + 4OH^- \rightarrow N_2 + 4H_2O + 4e^-$.

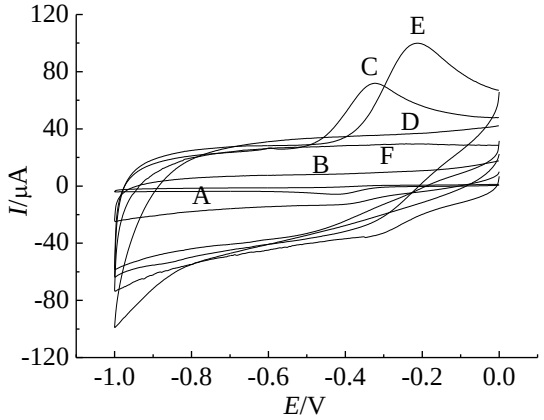

Figure 3. CVs on the GCE (A), rGO/GCE (B), Ag/rGO/GCE (C), and Ni/rGO/GCE (D) in the presence of 1.0 mM hydrazine; on the Ag-Ni/rGO/GCE electrode in the presence (E) and absence (F) of 1.0 mM hydrazine in 0.1 M NaOH. Scan rate: 0.05 V s^{-1}.

3.2. Effect of the Ag-Ni loading

The loading of Ag-Ni on the rGO can be changed by adjusting the electrodeposition cycles of Ag-Ni. In this work, the loading of Ag-Ni on the rGO can be expressed by the electrodeposition cycles. In Fig. 4, it can be seen that the hydrazine oxidation peak current changed with the electrodeposition cycles. When the electrodeposition cycles changed from 5 to 20, different hydrazine oxidation peak currents were obtained. When the number of electrodeposition cycles was 15, the peak current reached a maximum, which indicated the best laoding of Ag-Ni on the rGO. When the number of electrodeposition cycles was smaller, there were insufficient active sites for hydrazine electrocatalysis. When the number of electrodeposition cycles was above 15, the longer deposition time caused the nanoparticles to aggregate into larger particles or bundles, which negated the relative advantage of larger reactive surface area of smaller nanoparticles [39-41].

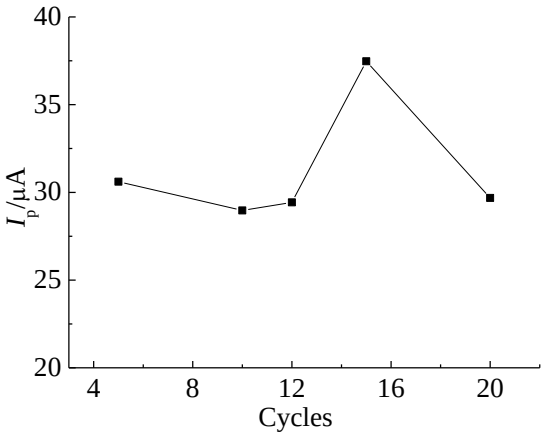

Figure 4. The peak currents for various electrodeposition cycles on the Ag-Ni/rGO/GCE with 1.0 mM hydrazine in 0.1 M NaOH.

3.3. Effect of the scan rate

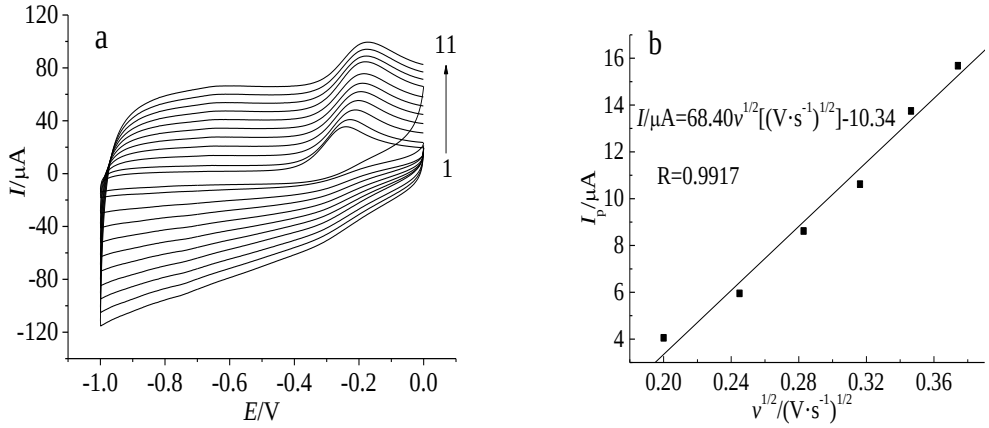

Figure 5. (a)The effect of scan rates on the Ag-Ni/rGO/GCE in 1.0 mM N_2H_4 (1 to 11: 20, 40, 60, 80, 100, 120, 140, 160, 180 and 200 mV·s^{-1}). (b) The plot of peak current versus $v^{1/2}$

The effect of the scan rate on the electrochemical oxidation of hydrazine was also explored. From Fig. 5, it can be seen that with the increase in the scan rate, the peak potentials shifted to more positive potentials which suggested that the oxidation of hydrazine was an irreversible electrochemical reaction [42]. From Fig. 5, it can also be seen that as the scan rate increased, the peak current increased. The peak current was proportional to the square root of scan rates, which indicated a diffusion-controlled process at the solution/electrode interface [42-44].

3.4. The determination of hydrazine

LSV was used to determine the concentration of hydrazine in Fig. 6a. The linear relation was in the hydrazine concentration range from 1.0 μM to 1.05 mM (Fig. 6b). The correlation coefficient was 0.9972 with a sensitivity of 28.42 μA mM^{-1} and a detection limit of 0.3 μM (*S*/*N*=3). The sensitivity of the proposed sensor was higher than that of sensors of previous reports [45-47]. The higher sensitivity might be due to the high electrocatalytic performance of the Ag-Ni/rGO composite.

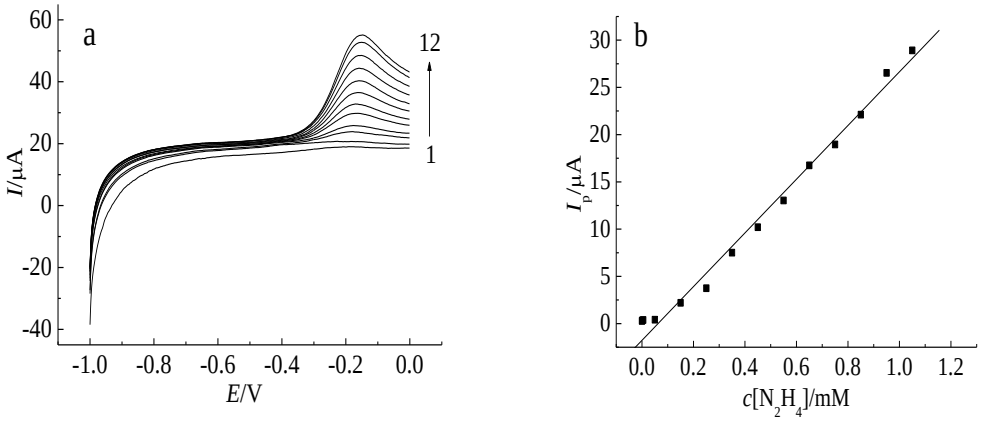

Figure 6. (a) LSV of different hydrazine concentrations on the Ag-Ni/rGO/GCE in 0.1 M NaOH (1 to 12: 0.001，0.05，0.15，0.25，0.35，0.45，0.55，0.65，0.75，0.85，0.95，1.05 mM at the scan rate of 50 $mV \cdot s^{-1}$). (b) The plot of peak current versus concentration of hydrazine.

Table 1. Comparison of different sensors for the determination of hydrazine

Electrode	Method	Linear range /μM	Detection limit /μM	Reference
CPE/PpDP/ZnO	CV	1000-60000	24	48
Nano-Au/Ti	LSV	500-4000	42	49
MWCNTs/Vitamin B12	Amperometry	2-1950	0.70	50
graphene/GCE	Amperometry	3.0-300	1.0	51
Pd/MWNT-Nafion/GCE	DPV	2.5-700	1.0	52
Ag/ZIF-8/CPE	Amperometry	6-5000	1.57	53
CoHCF-rGO/ GCE	Amperometry	0.25-100	0.069	54
Ag-Ni/rGO/GCE	LSV	1-1050	0.3	This work

Table 1 shows the comparison among the different hydrazine sensors. Table 1 shows that the hydrazine sensor based on the Ag-Ni/rGO composite has a lower detection limit than the previous reports [48- 53], and a wider linear range than the previous reports [51, 52, 54].

3.5. Reproducibility, stability and interference

The reproducibility, stability and interference of the hydrazine sensor based on the Ag-Ni/rGO composite were evaluated. The current response of six different hydrazine sensor based on the Ag-Ni/rGO composite was investigated in 0.1 mM hydrazine. The relative standard deviation (RSD) was 3.7%, which confirmed that the sensor was highly reproducible. Ten successive measurements using the same hydrazine sensor yielded a RSD of 4.1%, which indicated that the sensor was stable for repeated detection of hydrazine. When the catalytic current of the sensor was measured after 2 weeks, it retained approximately 87% of its original sensitivity, which showed that the long-term stability of the sensor was good. The influence of different substances as potential interfering compounds on the sensor selectivity was studied using 1.0 mM hydrazine in 0.1 M NaOH. The tolerance limit was the maximum concentration of the foreign substance, that caused an approximately ±5% relative error in the determination. The results showed that 100-fold quantities of common cations and anions (Na^+, K^+, ClO_4^-, Ni^{2+}, Ca^{2+}, Br^-, Zn^{2+}, Mg^{2+}, SO_4^{2-}, NO_3^-, NO_2^-) did not obviously interfere with the determination of hydrazine.

3.6. Application for real sample analysis

The hydrazine sensor based on the Ag-Ni/rGO composite was used for the determination of hydrazine in waste water samples in our laboratory. The results are summarized in Table 2. The results were satisfactory, which indicated that the hydrazine sensor based on the Ag-Ni/rGO composite could be applied for real sample analyses.

Table 2. Analytical results of hydrazine in waste water samples on the Ag-Ni/rGO/GCE

No.	Hydrazine added /μM	Hydrazine found[a] /μM	Recovery /%
1	50	51	102
2	100	103	103
3	150	153	101
4	200	197	99
5	300	298	99

(a.The result of average of three determinations by the sensor)

4. CONCLUSIONS

In this work, a hydrazine sensor was fabricated based on Ag-Ni/rGO composite. The Ag-Ni/rGO composite exhibited high electrocatalytic activity for the oxidation of hydrazine. Compared

with other previous reports on hydrazine determination, the hydrazine sensor based on the Ag-Ni/rGO composite showed a higher sensitivity of 28.42 μA mM^{-1} and a lower detection limit of 0.3 μM (S/N = 3) which can be ascribed to the synergetic effect of the Ag-Ni alloy and rGO.

Acknowledgments

This work was financially supported by Shaanxi Provincial Natural Science Foundation (No. 2013JQ2015), Scientific Research Program Funded by Shaanxi Provincial Education Department (No. 2013JK0673), Industrial research project of Science and Technology Department of Shaanxi Province (No. 2016GY-158).

References

1. S. Garrod, M.E.Bollard, A.W. Nicholls, S.C. Connor, J. Connelly, J. Nicholson and E. Holmes, *Chem. Res. Toxicol.*,18 (2005) 115.
2. S. M. Golabi and H. R. Zare, *J. Electroanal. Chem.* 465 (1999) 168.
3. J.W. Mo, B. Ogorevc, X. Zhang and B. Pihlar, *Electroanalysis* 12 (2000) 48.
4. S.J.R. Prabakar and S.S. Narayanan, *J. Electroanal. Chem.* 617 (2008) 111.
5. M. Mori , K. Tanaka, Q. Xu, M. Ikedo, H. Taoda and W. Hu, *J. Chromatogr.* A 1039 (2004) 135.
6. C. Gojon, B. Dureault, N. Hovnanian and C. Guizard, *Sens. Actuators*, B 38 (1997) 154.
7. J.S. Pinter, K.L. Brown, P.A. DeYoung and G.F. Peaslee, *Talanta* 71 (2007) 1219.
8. B. Liu, Y. He, C. Duan, N. Li and H. Cui, *J. Photochem. Photobiol.*, A, 217 (2011) 62.
9. U. Nickel, A. Z. Castell, K. Pöppl and S. Schneider, *Langmuir*, 16 (2000) 9087.
10. S.M. Golabi and H.R. Zare, *Electroanalysis* 11 (1999)1293.
11. C. Wang, L. Zhang, Z. Guo, J. Xu, H. Wang, K. Zhai and X. Zhuo, *Microchim. Acta* 69 (2010) 1.
12. Z. Yin, L. Liu and Z. Yang, *J. Solid State Electrochem.* 15 (2011) 821.
13. J. Yang, S. Deng, J. Lei, H. Ju and S. Gunasekaran, *Biosens. Bioelectron.* 29 (2011) 159.
14. D. Zheng, C. Hue, T. Gan, X. Dang and S. Hu, *Sens. Actuators*, B 148 (2010) 247.
15. J. Gong, T. Zhou, D. Song, L. Zhang and X. Hu, *Anal. Chem.* 82 (2010) 567.
16. C. Zhou, S. Li, W. Zhu, H. Pang and H. Ma, *Electrochim Acta* 113(2013)454.
17. Z. Yin, W. Zhou, Y. Gao, D. Ma, C.J. Kiely and X. Bao, *Chem. Eur. J.* 18 (2012) 4887.
18. Y. Bai, Y. Sun and C. Sun, *Biosens. Bioelectron.* 24 (2008) 579.
19. J.J. Huang, W.S. Hwang, Y.C. Weng and T.C. Chou, *Thin Solid Films* 516 (2008) 5210.
20. C.V. Rao, A.L.M. Reddy, Y. Ishikawa and P.M. Ajayan, *Carbon* 49 (2011) 931.
21. J. Yang, S. Deng, J. Lei, H. Ju and S. Gunasekaran, *Biosens. Bioelectron.* 29 (2011) 159.
22. L. Feng, G. Gao, P. Huang, X. Wang, C. Zhang, J. Zhang, S. Guo and D. Cui, *Nanoscale Res. Lett.* 6 (2011) 511.
23. C.Y. Tung, J.M. Gu, H.M. Lin, Y. Hwu and N.F. Cheng, *Nanostruct. Mater.* 9 (1997) 351.
24. N. Bhandary, A.P. Singh, S. Kumar, P.P. Ingole, G.S. Thakur, A.K. Ganguli and S. Basu, *ChemSusChem* 9 (2016) 2816.
25. Z. Zhang, T.M. Nenoff, J.Y. Huang, D.T. Berry and P.P. Provencio, *J. Phys. Chem.* C 113 (2009) 1155.
26. Z. Zhang, T. M. Nenoff, K. Leung, S. R. Ferreira, J. Y. Huang, D. T. Berry, P. P. Provencio and R. Stumpf, *J. Phys. Chem.* C, 114 (2010) 14309.
27. C. Srivastava, S. Chithra, K. D. Malviya, S. K. Sinha and K. Chattopadhyay, *Acta Mater.* 59 (2011) 6501.
28. S.William, J.R. Hummers and R. E. Offeman, *J. Am. Chem. Soc*. 80 (1958) 1339.
29. H.A. Becerril, J. Mao, Z. Liu, R.M. Stoltenberg, Z. Bao and Y. Chen, *ACS Nano* 2(2008) 463.
30. Y.G. Sun and Y.N. Xia, *Science* 298 (2002) 2176.

31. A. Lazzeri, S.M. Zebarjad, M. Pracella, K. Cavalier and R. Rosa, *polymer* 46 (2005) 827.
32. Z. Ji, X. Shen, G. Zhu, H. Zhou and A. Yuan, *J. Mater. Chem.* 22 (2012) 3471.
33. C. Srivastava, S. Chithra, K.D. Malviya, S.K. Sinha. and K. Chattopadhyay, *Acta Mater.* 59 (2011) 6501.
34. K. Santhi, E. Thirumal, S.N. Karthick, H.J. Kim, M. Nidhin, V. Narayanan and A. Stephen, *J. Nanopart. Res.*14 (2012) 1.
35. K. Sridharan, T. Endo, S.G. Cho, J. Kim, T.J. Park and R. Philip, *Opt. Mater.* 35(2013) 860.
36. M. Kumar and S. Deka, *ACS Appl. Mater. Interfaces* 6 (2014) 16071.
37. R. Dhanda and M. Kidwai, *J. Mater. Chem.* A 3 (2015) 19563.
38. J.B. Zheng, Q.L. Sheng, L. Li and Y. Shen, *J. Electroanal. Chem.* 61(2007)155.
39. J. Li and X.Q. Lin, *Sens. Actuators, B* 126 (2007) 527.
40. J. Yang, L.C. Jiang, W.D. Zhang and S. Gunasekaran, *Talanta* 82 (2010) 25.
41. J. Luo, S.S. Jiang, H.Y. Zhang, J.Q. Jiang and X.Y. Liu, *Anal. Chim. Acta* 709 (2012) 47.
42. N. Yusoff, P. Rameshkumar, M. S. Mehmood, A. Pandikumar, H. W. Lee and N. M. Huang, *Biosens. Bioelectron.* 87 (2017) 1020.
43. Y. Mu, D. Jia, Y. He, Y. Miao and H.L. Wu, *Biosens. Bioelectron.* 26 (2011) 2948.
44. M. Elancheziyan, D. Manoj, D. Saravanakumar, K. Thenmozhi and S. Senthilkumar, *Microchim. Acta* 184 (2017) 2925.
45. X. Li, S. Zhang and C. Sun, *J. Electroanal. Chem.* 553 (2003) 139.
46. H.R. Zare and A.M. Habibirad, *J. Solid State Electrochem.* 10 (2006) 348.
47. M. Revenga-Parra, E. Lorenzo and F. Pariente, *Sens. Actuators* B 107 (2005) 678.
48. H. Rostami, A. Omrani, A. A. Rostami and A. Emamgholizadeh, *Ionics* 21 (2015) 1073.
49. Q.F. Yi, W.Q. Yu, *J. Electroanal. Chem.* 633 (2009) 159.
50. Y. Umasankar, T.Y. Huang and S.M. Chen, *Anal. Biochem.* 408 (2011) 297.
51. C. Wang, L. Zhang, Z.H. Guo, J.G. Xu, H.Y. Wang, K.F. Zhai and X. Zhuo, *Microchim. Acta* 169 (2010) 1.
52. J.Y. Zhao, M.N. Zhu, M. Zheng, Y.W. Tang, Y. Chen and T.H. Lu, *Electrochim. Acta* 56 (2011) 4930.
53. S.M. Abdolraouf, G. Shahram and G.R. Hamid, *Sens. Actuators*, B, 220 (2015) 627.
54. X. Luo, J. Pan, K. Pan, Y.Yu, A. Zhong, S. Wei, J. Li, J. Shi and X. Li, *J. Electroanal. Chem.* 745(2015) 80.